Models for Concentration Fluctuations in Relative and Absolute Dispersion

R. J. Munro, P. C. Chatwin and N. Mole

Department of Applied Mathematics, University of Sheffield, Hicks Building, Sheffield S3 7RH, U.K.
(r.j.munro@sheffield.ac.uk)

Abstract: The relative dispersion of a contaminant plume (i.e. where the statistical description is relative to a coordinate system whose origin is the instantaneous centre of mass of the plume) is governed by the turbulence components of order of, and smaller than, the instantaneous dimension of the plume. Provided this dimension is characteristic of scales within the equilibrium range, the relative dispersion of the plume is expected to have a universal form. Presented here is a physically based model for the probability density function (pdf) of the contaminant concentration field within the relative framework. However, any practical model output is required in the absolute (or fixed) frame of reference. Hence, convolution techniques are used to transform the relative frame model into a corresponding absolute frame model. The accuracy of the results produced by these techniques is analysed and discussed.

Keywords: Absolute dispersion; Relative dispersion; Probability density function; Concentration fluctuations; Convolution

1. INTRODUCTION

Consider the steady continuous release of scalar contaminant into the turbulent atmospheric boundary-layer, and the subsequent dispersion of the resulting contaminant plume. The complex random structures inherent in turbulent flow, which occur over a wide range of temporal and spatial scales, vastly accelerate the effect of the comparatively slowly acting molecular diffusion process, producing increased rates of contaminant mixing and transport.

One important consequence of the wide spatial scale spectrum is that, in addition to the increasing plume dimension as the contaminant is transported downwind, the overall plume structure will also be subject to large scale meander. The turbulence components responsible for the meandering are predominantly the large energy containing components. The growth of the internal plume structure, however, is dominated by the turbulence scales of order of, and smaller than, the instantaneous plume dimension. Hence, provided attention is restricted to ranges so that the dimension of the plume is characteristic of scales within the equilibrium range [Batchelor, 1953], the relative dispersion of contaminant, about the centreline of the plume, will be dominated by the universal turbulence regime characteristic of the equilibrium range, which, in addition, is independent of the non-universal large scale turbulent components.

Consequently, statistical models for relative plume dispersion are likely to have an overall simpler structure than any corresponding model based in the fixed, or absolute, frame of reference. However, it is necessary for any practical model output or prediction to be given in the absolute framework. Hence, the main aim of this work is to develop statistical models for relative dispersion, and then use spatial convolution relationships, which relate the absolute and relative frame descriptions, to obtain absolute frame models.

The dispersion process was first modelled using these techniques by Gifford [1959], who developed a meandering plume model in which concentration fluctuations were due solely to

the large scale meandering of the plume. This idea has since been extended, and more realistic physical models in which internal fluctuations are also included, have been analysed; for example see Reynolds [2000], and Yee and Wilson [2000].

2. NOTATION

Let $\Gamma(\boldsymbol{X},t)$ denote the contaminant concentration field at position $\boldsymbol{X}$, relative to the source position, and time t, where X_1 is aligned in the downwind direction, and X_3 is directed vertically upwards. At each time t, let $\boldsymbol{R}(X_1,t) = (X_1, R_2(X_1,t), R_3(X_1,t))$ be the position vector of the instantaneous plume centreline at the downwind distance X_1, where

$$(R_2,R_3) = Q^{-1}\iint_{\mathbb{R}^2}(X_2,X_3)\,\Gamma(\boldsymbol{X},t)\,dX_2\,dX_3, \tag{1}$$

and $Q(X_1,t)$ is given by

$$Q = \iint_{\mathbb{R}^2}\Gamma(\boldsymbol{X},t)\,dX_2\,dX_3. \tag{2}$$

At each downwind location X_1, it is now possible to define the coordinate system relative to the instantaneous plume centreline position, which will be denoted by $\boldsymbol{x}$ and defined by

$$\boldsymbol{x} = (0,x_2,x_3) = \boldsymbol{X} - \boldsymbol{R}, \tag{3}$$

where $x_2 = X_2 - R_2$ and $x_3 = X_3 - R_3$. Then, for each relative position $\boldsymbol{x}$ and time t, let $\Gamma_r(\boldsymbol{x},t)$ be the concentration field relative to the plume centreline position $\boldsymbol{R}(X_1,t)$, which is related to $\Gamma(\boldsymbol{X},t)$ by

$$\Gamma_r(\boldsymbol{x},t) = \Gamma(\boldsymbol{x}+\boldsymbol{R},t). \tag{4}$$

Since $\Gamma(\boldsymbol{X},t)$, $\Gamma_r(\boldsymbol{x},t)$ and $\boldsymbol{R}(X_1,t)$ are random variables, the only reproducible properties will be statistical quantities, definitions of which will be given subsequently. First, note that consideration is restricted to dispersion periods much less than the timescale on which meteorological conditions vary. Consequently, since contaminant is continuously released at a steady rate, Γ, Γ_r and $\boldsymbol{R}$ can be considered as stationary random variables. Hence, let $p_\Gamma(\theta;\boldsymbol{X})$ and $p_{\Gamma_r}(\theta;\boldsymbol{x})$ denote the pdfs of $\Gamma(\boldsymbol{X},t)$ and $\Gamma_r(\boldsymbol{x},t)$ respectively, which can then be used to define the usual statistical quantities. For example, in the absolute framework, the mean concentration $C(\boldsymbol{X})$, central moments $M^{(n)}(\boldsymbol{X})$, and standard moments $m^{(n)}(\boldsymbol{X})$ are defined by

$$\begin{aligned} C(\boldsymbol{X}) &= \int_{\mathbb{R}}\theta\,p_\Gamma(\theta;\boldsymbol{X})\,d\theta,\\ M^{(n)}(\boldsymbol{X}) &= \int_{\mathbb{R}}(\theta-C)^n\,p_\Gamma(\theta;\boldsymbol{X})\,d\theta, \qquad (5)\\ m^{(n)}(\boldsymbol{X}) &= \int_{\mathbb{R}}\theta^n\,p_\Gamma(\theta;\boldsymbol{X})\,d\theta. \end{aligned}$$

The corresponding relative framework moments $C_r(\boldsymbol{x})$, $M_r^{(n)}(\boldsymbol{x})$ and $m_r^{(n)}(\boldsymbol{x})$ are defined similarly.

The absolute frame pdf $p_\Gamma(\theta;\boldsymbol{X})$ is related to the relative frame pdf $p_{\Gamma_r}(\theta;\boldsymbol{x})$ by the convolution relation

$$p_\Gamma(\theta;\boldsymbol{X}) = \iint_{\mathbb{R}^2}p_{\Gamma_r}(\theta;\boldsymbol{x})\,p_{\boldsymbol{R}}(\boldsymbol{X}-\boldsymbol{x})\,dx_2dx_3, \tag{6}$$

where $p_{\boldsymbol{R}}$ is the pdf of the plume centreline position. The relationships for the standard moments can be obtained directly from (6), i.e.

$$m^{(n)}(\boldsymbol{X}) = \iint_{\mathbb{R}^2}m_r^{(n)}(\boldsymbol{x})\,p_{\boldsymbol{R}}(\boldsymbol{X}-\boldsymbol{x})\,dx_2dx_3. \tag{7}$$

3. RELATIVE FRAME ANALYSIS

The concentration measurements used in the analysis were obtained in a series of atmospheric release experiments (the Madona field trials; full specifications given in Mikkelsen et al. [1995]). The release contaminant was an artificial smoke consisting of small particles, and concentration measurements were obtained using a Lidar [Jørgensen et al., 1997] fired horizontally across the smoke plume, and normal to the mean wind direction. Lidar systems provide instantaneous concentration measurements at many crossplume locations (at 3 m intervals), so are ideal for using in relative framework analysis.

Since Lidar measurements are obtained in a horizontal line across the plume, and at a fixed downwind location, the analysis is restricted to the following one-dimensional situation. Let y denote the absolute framework coordinate along the line-of-sight of the Lidar, and $\Gamma(y,t)$ denote the corresponding concentration field. Then previous definitions can be modified as appropriate.

In particular, (1) and (2) reduce to

$$R(t) = Q^{-1}\int_{\mathbb{R}}y\,\Gamma(y,t)\,dy, \tag{8}$$

$$Q(t) = \int_{\mathbb{R}}\Gamma(y,t)\,dy. \tag{9}$$

Measurements of $R(t)$ were obtained from the data, and then $p_{\boldsymbol{R}}(y)$ was estimated using kernel density estimation [Roussas, 1997] with a

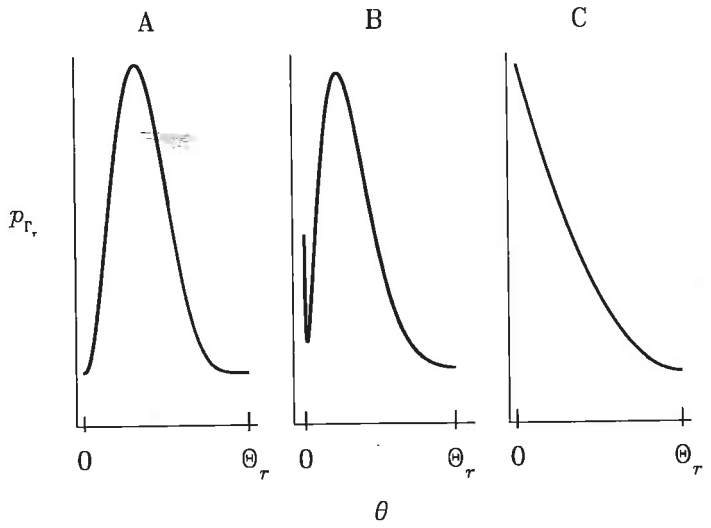

Figure 1. Schematic showing the range of shapes of $p_{\Gamma_r}(\theta; x)$ observed in the data.

Gaussian kernel. As expected, these estimates indicate that the variability of R increases with downwind distance.

Gifford [1959] assumed $p_R(y)$ to be Gaussian, which is a reasonable assumption if the turbulence is homogeneous in the y-direction. Also, Yee and Wilson [2000] present a mathematical argument to show that $p_R(y)$ is Gaussian if dispersion is symmetric in the y-direction. Hence, fits were obtained by assuming a Gaussian form for p_R, i.e.

$$p_R(y) = \frac{1}{\sqrt{2\pi}\sigma_R} \exp\left(-\frac{(y-\mu_R)^2}{2\sigma_R^2}\right), \quad (10)$$

where the mean μ_R, and standard deviation σ_R, of R, were estimated from the data. The fits compared well with the kernel density estimates. Since meander is dominated by large scale motions, one expects convergence of estimates of p_R to be relatively slow, so the differences are probably not significant.

The absolute framework measurements were used to generate relative frame measurements at intervals of 3 m (approximately twice the spatial resolution of the Lidar) relative to the centreline position R. Analysis of these revealed three possible shapes for the pdf $p_{\Gamma_r}(\theta; x)$ of $\Gamma_r(x,t)$, where $x = y - R$ is the relative frame coordinate, which are shown in figure 1. (Note that Θ_r denotes the ensemble maximum concentration.)

The overall physical picture obtained from this analysis can be summarized as follows. At downwind locations relatively close to the source, where there has been little time for molecular diffusion to act, the type A pdf will be observed around $x = 0$, with a transition into type C as $|x|$ increases; this process is likely to include an intermediate transition into type B. Very far downwind, where there has been a long time for material to diffuse into entrained ambient air, one would observe type C at all x across the plume. At intermediate downwind locations, the most likely structure would be a transition from type B to C with increasing $|x|$. Furthermore, in all cases, Θ_r was maximum around $x = 0$, and decreased with increasing $|x|$, and all structures were found to be essentially symmetric about $x = 0$.

Attention now centres on developing simple parametric model pdfs capable of producing types A, B and C, which also satisfy necessary underlying physical constraints. For example, $p_{\Gamma_r}(\theta; x)$ has finite support $(0, \Theta_r)$, where $\Theta_r = \Theta_r(x)$, i.e $p_{\Gamma_r}(\theta; x) = 0 \forall \theta \notin (0, \Theta_r)$. There are also asymptotic conditions on $p_{\Gamma_r}(\theta; x)$; for example, $p_{\Gamma_r}(\theta; x) \to \delta(\theta)$ as $|x| \to \infty$ (i.e. $\Theta_r \to 0$ as $|x| \to \infty$). It has also been shown [Chatwin and Sullivan, 1989, 1990] that $p_{\Gamma_r}(\theta; x)$ (and $p_r(\theta; y)$) can be written exactly as the weighted sum of two component pdfs, where the individual components have a precise physical definition. i.e. the probability that the fluid element at x and time t has, or has not, emanated from the source.

A number of possible pdfs have been considered, the most successful of which was such a mixture distribution, with a generalized Pareto distribution (GPD) and a beta distribution as components. This pdf will be denoted by BGPD, and is given by

$$p_{\Gamma_r}(\theta;x) = \gamma(x) f_1(\theta;x) + [1-\gamma(x)] f_2(\theta;x), \tag{11}$$

where

$$f_1(\theta;x) = \frac{1}{\xi_1}\left(1-\frac{\theta}{\Theta_r}\right)^{\xi_2-1} \tag{12}$$

$$f_2(\theta;x) = \frac{1}{\Theta_r B(\eta_1,\eta_2)}\left(\frac{\theta}{\Theta_r}\right)^{\eta_1-1}\left(1-\frac{\theta}{\Theta_r}\right)^{\eta_2-1} \tag{13}$$

and $\xi_1, \xi_2, \eta_1 > 0$, $\eta_2 > 1$, $0 \leqslant \gamma \leqslant 1$. Also, $\Theta_r = \xi_1\xi_2$, and is the same in each component, so that the BGPD has five independent parameters. Maximum likelihood (**ML**) [Roussas, 1997] was used to fit the BGPD to the relative framework data; an example of the fits produced, compared with histograms generated from the data, is given in figure 2 (note that $\wedge$ will be used throughout to denote an estimate of a quantity). The BGPD produced good fits to all the datasets, and at all locations x considered.

At locations x where the type A pdf was observed, the f_2 component dominates (i.e. $\hat{\gamma} \approx 0$). However, when type B is observed, $0.1 \leqslant \hat{\gamma} \leqslant 0.2$ and so the f_1 component makes an essential contribution to the mode at $\theta = 0$. Furthermore, in some experiments $\hat{\gamma}$ increased towards the plume edges where the type C pdf was observed, and so the f_2 component can also make a significant contribution at these plume edge locations.

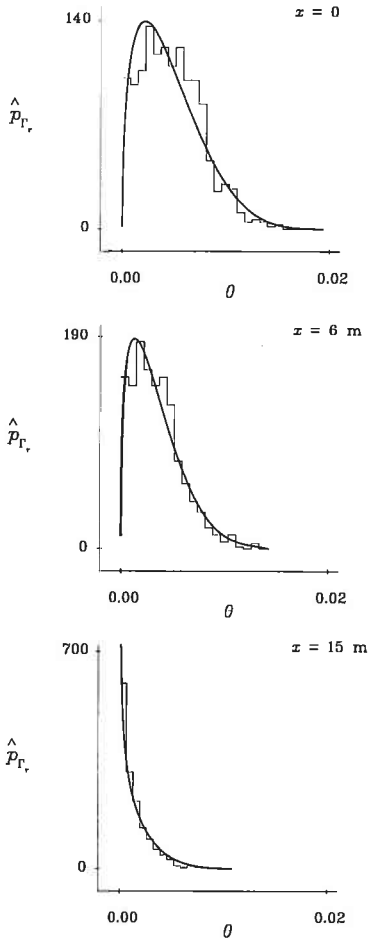

Figure 2. Examples of the maximum likelihood fits obtained for the BGPD defined by (11)–(13), compared with the corresponding histogram, at relative positions $x = 0$, $x = 6\,\mathrm{m}$ and $x = 15\,\mathrm{m}$. This data (mad14h) was obtained relatively close to the source, at a downwind distance 230 m.

4. ABSOLUTE FRAME ANALYSIS

Firstly, the one-dimensional forms of (6) and (7) are

$$p_r(\theta;y) = \int_{\mathbb{R}} p_{\Gamma_r}(\theta;x)\, p_R(y-x)\, dx, \tag{14}$$

$$m^{(n)}(y) = \int_{\mathbb{R}} m_r^{(n)}(x)\, p_R(y-x)\, dx. \tag{15}$$

The fitted Gaussian for $p_R(y)$ and the BGPD for $p_{\Gamma_r}(\theta;x)$ were then used to model $p_r(\theta;y)$.

For given values of θ and y the right-hand side of (14) was evaluated using the trapezoidal rule with values of the integrand at the values of x for which p_{Γ_r} was estimated. An example of the fits produced using this procedure (for the same data used to obtain the figure 2 fits), compared against histograms obtained from the absolute framework measurements, is given in figure 3. Except at small θ the fits are generally very good. This deterioration in the fit, at small θ, can be explained as follows.

The estimates for p_{Γ_r} have been obtained over a finite interval of x, i.e. $|x| \leqslant L$, where, for example, $L = 36\,\mathrm{m}$ for the data used to obtain the fits in figure 2. Now, let $\Theta_{\min} = \min\{\hat{\Theta}_r(x)\}$, and recall that $\hat{\Theta}_r(x)$ decreased as $|x|$ increased. Hence, for $\theta > \Theta_{\min}$ we have estimates of all non-zero values of $p_{\Gamma_r}(\theta;x)$. However, for $\theta < \Theta_{\min}$ this is not the case; and as θ decreases towards zero an increasing range of non-zero contributions to (14) will fall outside $-L \leqslant x \leqslant L$, and so will not be included in the approximation to the right-hand side of (14). This problem will also become worse as $|y - \hat{\mu}_R|$ increases, since $p_R(y-x)$ gives increasing weight to the missing contributions to $p_{\Gamma_r}(\theta;x)$. Thus, even if our models for $p_{\Gamma_r}(\theta;x)$ and $p_R(y)$ are very good, we expect decreasing accuracy for the resultant $p_r(\theta;y)$ model as θ decreases below $\Theta_{\min}$ and $|y - \hat{\mu}_R|$ increases.

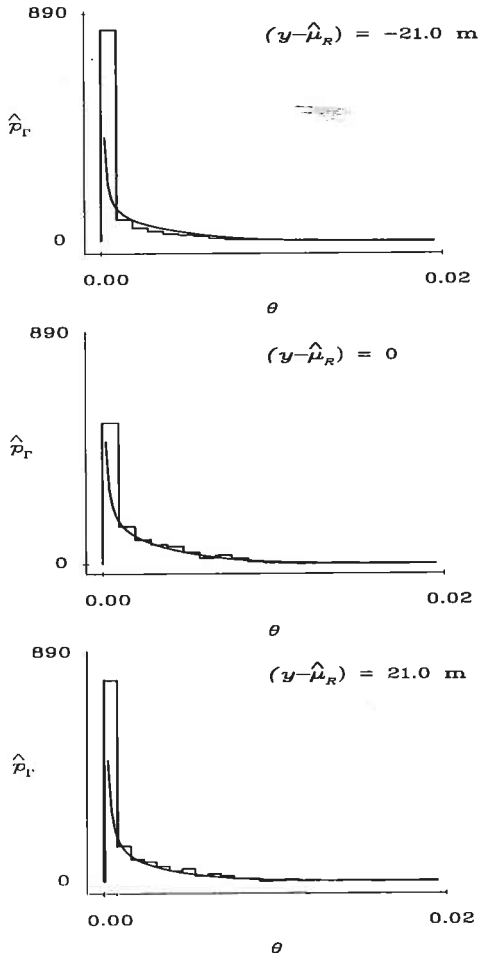

Figure 3. Results of the convolution (14) compared against the histograms plotted from the absolute frame measurements, using the same data set (mad14h) used to obtain the fits in figure 2. Note that, for this data, $\Theta_{\min} \approx 0.004$.

The fitted Gaussian for $p_R(y)$, and the values of $m_r^{(1)}(x)$ and $m_r^{(2)}(x)$ obtained directly from the relative frame measurements, were then used to model $m^{(1)}(y)$ and $m^{(2)}(y)$ using (15). A similar numerical approximation procedure to the one described above was used. Figure 4 shows the results of this procedure applied to the dataset used for the previous plots, along with (for illustration) the values of $m_r^{(1)}(x)$ and $m_r^{(2)}(x)$ used in the procedure (broken curve). This procedure also produces good results, but similarly, we expect accuracy to decrease as $|y - \hat{\mu}_R|$ increases, albeit with a lesser effect since we expect the necessary limiting condition $m_r^{(n)}(x) \to 0$ as $|x| \to \infty$ to be attained at relatively short ranges of $|x|$ (as is illustrated in figure 4).

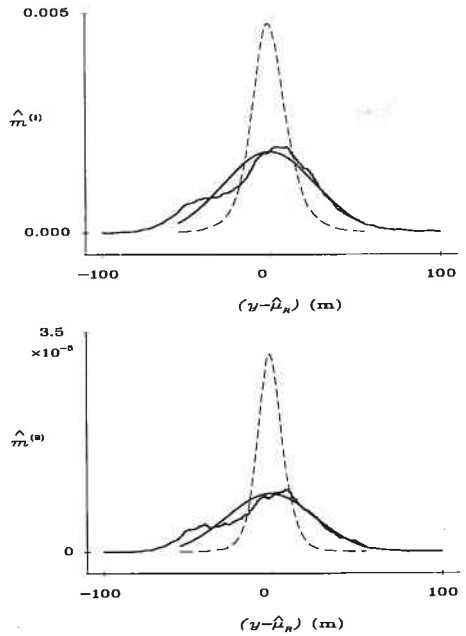

Figure 4. Results of the convolution (15) (smooth curve) compared against the moments obtained from the absolute frame data (again using the mad14h dataset). Also shown is the values of $m_r^{(1)}(x)$ and $m_r^{(2)}(x)$ used in the convolution procedure (broken curve).

5. DISCUSSION

The inaccuracy problem associated with the approximation for the pdf convolution (14) can be overcome by modelling the parameters of $p_{\Gamma_r}(\theta; x)$ for all $x \in \mathbb{R}$, which would include modelling the approach of p_{Γ_r} to the limit $\delta(\theta)$. Of course, due to the finite range of the measurements, this would involve a degree of subjectivity for large values of $|x|$ where data is not available. Given the smooth symmetric forms of the estimated values of $m_r^{(1)}(x)$ and $m_r^{(2)}(x)$ obtained from the measurements, a model based on the moment convolution (15) should be much simpler to implement.

Presented above is the results of determining the parameter values by fitting (11)-(13) to data. To use the BGPD as part of a model for concentration fluctuations it would be necessary to supply a model for the dependence of parameters on relative position, downwind location, atmospheric and source conditions, etc.

6. ACKNOWLEDGEMENTS

This work was supported by the EU funded COFIN project, contract number ENV4-CT97-0629. We would also like to thank our project

partners at Risø National Laboratory, Denmark, for their help.

7. REFERENCES

Batchelor, G. K., *The Theory of Homogeneous Turbulence*, Cambridge University Press, 1953.

Chatwin, P. C., and P. J. Sullivan, The intermittency factor of scalars in turbulence, *Physics of Fluids A*, 1, 761–763, 1989.

Chatwin, P. C., and P. J. Sullivan, A simple and unifying physical interpretation of scalar fluctuation measurements from many turbulent shear flows, *Journal of Fluid Mechanics*, 212, 533–556, 1990.

Gifford, F., Statistical properties of a fluctuating plume dispersion model, *Advances in Geophysics*, 6, 117–137, 1959.

Jørgensen, H. E., T. Mikkelsen, J. Streicher, H. Herrmann, C. Werner, and E. Lyck, Lidar calibration experiments, *Applied Physics B*, 64, 355–361, 1997.

Mikkelsen, T., H. E. Jørgensen, S. Thykier-Nielsen, S. W. Lund, and J. M. Santabarbara, Final data and analysis report on: high-resolution in plume concentration fluctuations measurements using Lidar remote sensing technique, Technical Report Risø-R-852(EN), Risø National Laboratory, Roskilde, Denmark, 1995.

Reynolds, A. M., Representation of internal plume structure in Gifford's meandering plume model, *Atmospheric Environment*, 34, 2539–2545, 2000.

Roussas, G. G., *A Course in Mathematical Statistics*, Second Edition, Academic Press, 1997.

Yee, E., and D. J. Wilson, A comparison of the detailed structure in dispersing tracer plumes measured in grid-turbulence with a meandering plume model incorporating internal fluctuations. *Boundary-Layer Meteorol.*, 94, 253–296, 2000.